# *Highly Selective Cu-Modified $Ni/SiO_2$–$Al_2O_3$ Catalysts for the Conversion of Maleic Anhydride to γ-Butyrolactone in Gas Phase*

**M. E. Bertone, S. A. Regenhardt, C. I. Meyer, V. Sebastian, T. F. Garetto & A. J. Marchi**

**Topics in Catalysis**

ISSN 1022-5528
Volume 59
Combined 2-4

Top Catal (2016) 59:159-167
DOI 10.1007/s11244-015-0424-7

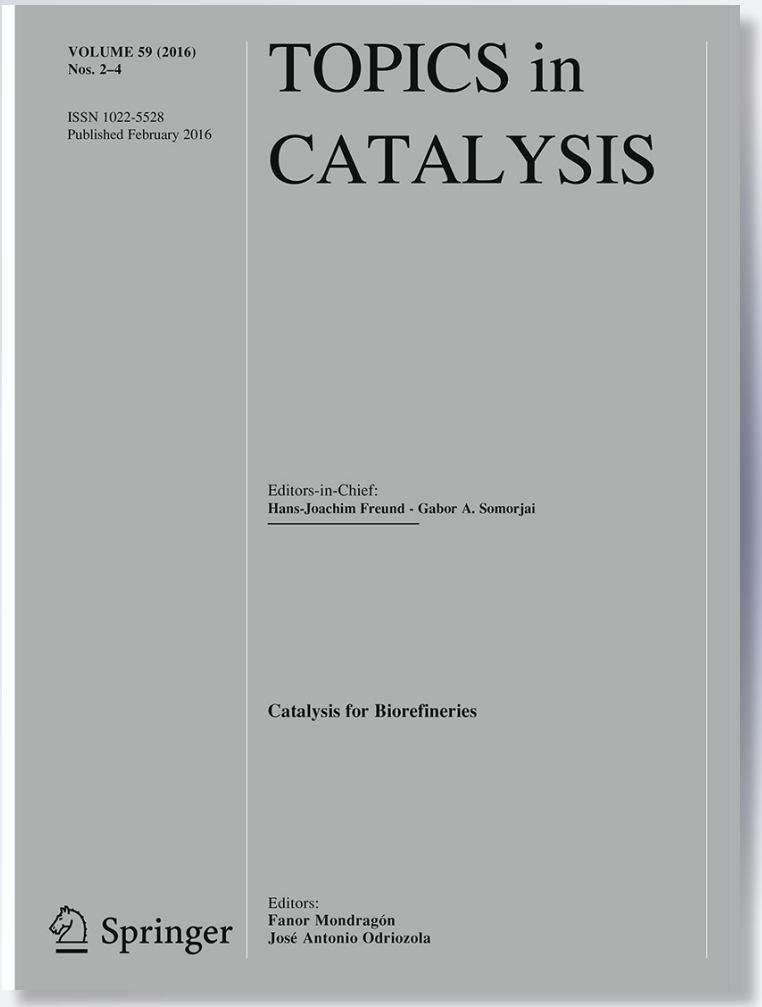


Springer

Top Catal (2016) 59:159–167
DOI 10.1007/s11244-015-0424-7

ORIGINAL PAPER

# Highly Selective Cu-Modified Ni/$SiO_2$–$Al_2O_3$ Catalysts for the Conversion of Maleic Anhydride to γ-Butyrolactone in Gas Phase

**M. E. Bertone[1] · S. A. Regenhardt[1] · C. I. Meyer[1] · V. Sebastian[2,3] · T. F. Garetto[1] · A. J. Marchi[1]**

Published online: 30 July 2015


**Abstract** The gas phase hydrogenation of maleic anhydride (MA) to succinic anhydride (SA) and the subsequent hydrogenolysis to γ-butyrolactone (GBL) was studied on $SiO_2$–$Al_2O_3$-supported Ni catalysts modified with Cu and prepared by incipient wetness impregnation (Ni-I, CuNi-I) and coprecipitation-deposition (CuNi-PD) methods. The samples were characterized by $N_2$ adsorption at −196 °C, X-ray diffraction, temperature-programmed reduction, transmission electron microscopy and $H_2$ chemisorption. Catalytic tests were performed between 170 and 220 °C at atmospheric pressure in a fixed bed reactor. Crystalline NiO along with a $Ni^{2+}$ phase strongly interacting with the support was observed in the oxide precursors. The extent of the strongly interacting $Ni^{2+}$ phase diminishes according to the following pattern: CuNi-PD > CuNi-I > Ni-I, along with a proportional rise of the NiO phase. The proportion of small to large metal particles, formed after reduction, followed the same pattern as that observed for the extent of $Ni^{2+}$ phase. All catalysts were very active in the MA hydrogenation to SA, but displayed distinct performances with respect to the subsequent SA hydrogenolysis. Hydrogenolytic activity and GBL yield increased following the same pattern as that obtained for the extent of $Ni^{2+}$ phase. In addition, the effect of raising temperature on hydrogenolytic activity was more important in the case of Ni-I and CuNi-I than for CuNi-PD. Furthermore, CuNi-PD was more selective to GBL than CuNi-I. These results showed that there is an important effect of Cu addition and preparation method on both the structure and catalytic performance of the metal Ni phase.

**Keywords** Selective hydrogenation · Maleic anhydride · γ-Butyrolactone · Cu–Ni catalysts · Precipitation-deposition method

## 1 Introduction

The gas phase hydrogenation of maleic anhydride (MA) is an important process to obtain succinic anhydride (SA), γ-butyrolactone (GBL), tetrahydrofurane (THF), 1,4-butanediol (BDO) and propionic acid (PA). These compounds, GBL, THF and BDO, are widely used intermediates in the chemical industry and mainly employed as solvents, especially to replace non eco-friendly chlorinated solvents such as trichloroethane. Particularly, GBL is used in the synthesis of pyrrolidone and N-methylpyrrolidone, which are employed in the production of agrochemicals, pharmaceuticals and polymers [1–3].

The gas-phase hydrogenation of MA reaction was studied using several types of noble metal-based catalysts, such as Pd, Pt and Au, as well as Cu-based catalyst, both in liquid and gas phase [3–14]. Generally, the experiments were performed at temperatures between 190 and 240 °C and pressures between 1 and 5 MPa. Particularly, Cu-based catalysts were used to study the gas-phase hydrogenation of MA between 210 and 280 °C [6–9, 14]. In general, the

✉ A. J. Marchi
amarchi@fiq.unl.edu.ar;
http://www.fiq.unl.edu.ar/gicic

[1] Catalysis Science and Engineering Research Group (GICIC), INCAPE, UNL-CONICET, Colectora Ruta Nac. N° 168 Km. 0 – Paraje El Pozo, 3000 Santa Fe, Argentina

[2] Department of Chemical Engineering, Aragon Institute of Nanoscience (INA), University of Zaragoza, Campus Río Ebro-Edificio I+D, C/Poeta Mariano Esquillor S/N, 50018 Saragossa, Spain

[3] CIBER de Bioingeniería, Biomateriales y Nanomedicina (CIBER-BBN), Campus Río Ebro-Edificio I+D, 50018 Saragossa, Spain

catalysts composition of these Cu-based catalysts is rather complex since they also contain Al, Zn, Cr and/or Ce. In addition, the use of Cr-containing catalysts is undesirable because of its toxicity. In some cases, catalyst deactivation has been reported for copper-based catalysts [14–16].

It was already shown that Ni-based catalysts prepared by incipient wetness impregnation were active and stable when they were tested in the gas phase MA hydrogenation and subsequent SA hydrogenolysis at atmospheric pressure [17–19]. Additionally, the effect of the support used on these Ni-based catalysts was studied, finding that $SiO_2$–$Al_2O_3$ was the most stable and selective to obtain GBL [18]. Moreover, it was shown that the optimum Ni metal load to obtain GBL was 10 % when $SiO_2$–$Al_2O_3$ was used as a support [19]. It was also found that the reaction scheme over Ni catalysts involves the selective hydrogenation of MA to SA, followed by hydrogenolysis of SA to give GBL and/or PA along with CO. Finally, GBL may be converted by hydrogenolysis to PA and $CH_4$ [17].

In addition to incipient wetness impregnation, precipitation-deposition is a widely known method that can be used to apply an active metal on a support. This method has the advantage of being able to produce catalysts with a stronger metal-support interaction and smaller metal particle size than incipient wetness impregnation [20, 21].

In this work, we prepared Cu–Ni/$SiO_2$–$Al_2O_3$ bimetallic catalysts (Ni:Cu mass ratio of 19) by incipient wetness impregnation and constant-pH coprecipitation-deposition methods. The main objective was to analyse the influence of adding small amounts of Cu to Ni using different preparation methods, on the catalytic behaviour of metal Ni supported on $SiO_2$–$Al_2O_3$ for the gas-phase MA hydrogenation to GBL. The performance of the Cu–Ni/$SiO_2$–$Al_2O_3$ bimetallic catalysts obtained is compared with that of a Ni/$SiO_2$–$Al_2O_3$ catalyst prepared by incipient wetness impregnation.

## 2 Experimental

### 2.1 Catalysts Preparation

Silica-Alumina (Sigma-Aldrich Grade 135, $S_g = 467$ $m^2$ $g^{-1}$, $V_p = 0.67$ $cm^3$ $g^{-1}$, $d_p = 5.54$ nm) was calcined in air at 500 °C during 4 h previous to its use as a catalyst support. Depending on the preparation method, catalyst precursors were prepared using aqueous solutions of $Ni(NO_3)_2$ (Anedra, 98 %) and $Cu(NO_3)_2$ (Merck, 99.9 %) with the exact concentration to obtain a theoretical total metal loading of 10 % by weight.

A monometallic Ni/$SiO_2$–$Al_2O_3$ sample and a bimetallic Cu–Ni/$SiO_2$–$Al_2O_3$ sample were prepared by incipient wetness impregnation and they were named Ni-I and CuNi-I, respectively. Another bimetallic Cu–Ni/$SiO_2$–$Al_2O_3$ sample was prepared by the constant-pH coprecipitation-deposition method and named as CuNi-PD. Ni-I sample was prepared by adding dropwise the necessary volume of a 1.1 M aqueous solution of $Ni(NO_3)_2$ to the support. A similar procedure was used to prepare CuNi-I sample but now a solution containing both $Ni(NO_3)_2$ and $Cu(NO_3)_2$, with a 1.1 M total concentration and a Ni:Cu mass ratio of 19, was added drop by drop to the support.

CuNi-PD sample was prepared using a mixed $Ni(NO_3)_2$ and $Cu(NO_3)_2$ aqueous solution, 0.4 M total concentration and Ni:Cu mass ratio of 19, and a 0.5 M $K_2CO_3$ solution as the precipitating agent. Solutions were added simultaneously to a mechanically stirred suspension of the support in deionized water, maintaining the pH at 7.2 ± 0.2 and the temperature at 65 ± 0.5 °C.

Both the impregnated and coprecipitated samples were dried overnight at 90 °C and then calcined in air at 500 °C for 2 h. Finally, the activation was carried out in situ under $H_2$ flow as described in Sect. 2.3.

### 2.2 Catalysts Characterization

Elemental compositions were measured by inductively coupled plasma (ICP), using a Perkin Elmer Optima 2100 DV spectrometer. The specific surface area (*Sg*), pore volume (*Vp*) and mean pore diameter (*dp*) of the calcined samples were measured by $N_2$ physisorption at −196 °C, with a Quantachrome Accusorb S-1 sorptometer. *Sg* was estimated by employing the BET equation and the pore distribution was determined by applying the BJH method. Previously to $N_2$ physisorption, samples were degassed under vacuum at 250 °C.

The crystalline species present in the calcined samples were identified by X-ray diffraction (XRD), in the 2θ range of 10°–80° at a scan speed of 2° $min^{-1}$, using a Shimadzu D1 diffractometer and Ni-filtered Cu-Kα radiation (λ = 0.1540 nm). Crystallites size were calculated from the NiO (0 1 2) diffraction lines using the Scherrer equation. Temperature programmed reduction (TPR) profiles were obtained in a Micromeritics AutoChem 2920 system, equipped with a TCD detector. The sample (100 mg) was heated from 25 to 800 °C at 10 °C $min^{-1}$ under $H_2$(5 %)/Ar with a volumetric flow rate of 60 mL STP $min^{-1}$.

The hydrogen chemisorption capabilities were determined by volumetric adsorption experiments at 25 °C in a conventional vacuum unit equipped with an MKS Baratron pressure gauge. Catalysts were previously reduced in situ at 500 °C for 2 h and then outgassed 2 h at 500 °C prior to performing $H_2$ chemisorption experiments. Hydrogen uptake was determined using double isotherm method. The amount of irreversibly chemisorbed $H_2$ was calculated as the difference between total and weakly adsorbed $H_2$.

Transmission electron microscopy (TEM) images were obtained using a 200 kV G2 20 S-Twin Tecnai microscope with a $LaB_6$ electron source. Previously, the samples were reduced ex situ under $H_2$ (100 %) flow at 500 °C for 1 h, cooled to room temperature in $N_2$ flow and then passivated sweeping with an $O_2$ (2 %)/$N_2$ stream. Then, catalyst powder was dispersed in milli-Q water. After 30 s in an ultrasonic bath, a drop of this suspension was applied to a copper grid (200 mesh) coated with carbon film, and allowed to dry in air.

### 2.3 Catalytic Tests

Catalytic activity tests were carried out at atmospheric pressure in a stainless steel fixed-bed tubular reactor (i.d. 10 mm) operated in down flow mode. Calcined precursors samples were pressed to obtain tablets that were then crushed and screened. The fraction in the 0.35–0.42 mm range was loaded into the reactor after dilution with quartz. Catalyst loading (W) of 0.05 g, contact time $\left(W/F^0_{AM}\right)$ of 12 g h $mol^{-1}$ and gas flow rate of 150 $cm^3$ $min^{-1}$ were used for catalytic tests. Under these experimental conditions, the flow regime was turbulent (Re > 10.000). Experiments were carried out at 170, 195 and 220 °C after in situ activation of the samples in pure $H_2$ flow (100 $cm^3$ $min^{-1}$) at 500 °C for 1 h. The reactor effluent was analyzed by on-line gas chromatography using a Varian CP 3380 gas chromatograph equipped with flame ionization detector and a Graphpac GC 0.1 % AT-1000 (80–100) packed column.

## 3 Results and Discussion

### 3.1 Physicochemical Characterization

The composition and textural properties of the prepared and calcined samples are shown in Table 1. The total metal loadings and Cu:Ni ratios determined by ICP are in good agreement with theoretical values. The *Sg*, *Vp* and *dp* of oxide precursors, i.e. samples after calcination, were quite similar to that of the original support. The most important diminution of *Vp* and *dp* respect to the original support was around 20 % and it was observed for CuNi-PD sample. Thus, it can be considered that the main textural properties of $SiO_2$–$Al_2O_3$ were not significantly affected by the preparation methods.

The X-ray diffractograms (XRD) of the oxide precursors are shown in Fig. 1. In all of the samples, the amorphous $SiO_2$–$Al_2O_3$ halo was observed between $2\theta = 10°$ and 35°. In addition, diffraction peaks at $2\theta = 37.3°$, 43.4°, 63.1° and 75.7° were clearly observed for both samples prepared by impregnation (Fig. 1A, B). These peaks can be assigned to a polycrystalline NiO phase (PDF-2-44-1159) formed on the surface of the $SiO_2$–$Al_2O_3$ used as a support. However, it is important to notice that the peak intensities are much lower in the case of the CuNi-I sample than for the

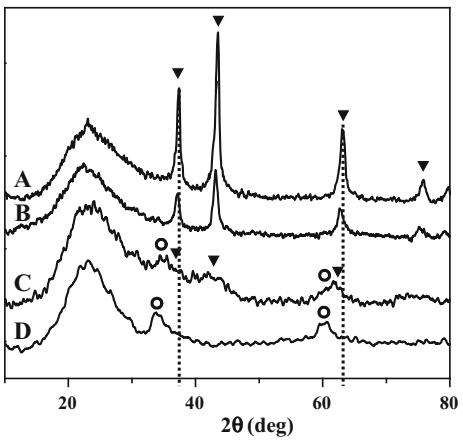


**Fig. 1** X-ray diffractograms of samples calcined in air at 500 °C (*A* Ni-I; *B* CuNi-I, *C* CuNi-PD) and hydrated precursor of CuNi-PD (*D*). *Filled down pointing triangle* NiO (PDF-2-44-1159), *open circle* Ni antigorite-like phase ($Ni_3Si_2O_5(OH)_4$, PDF-2-22-0754)

**Table 1** Composition and textural properties of the calcined samples

| Sample | ML (w%)[a] | $S_g$ ($m^2$ $g^{-1}$)[b] | $V_P$ ($cm^3$ $g^{-1}$)[b] | $d_P$ (nm)[b] | L (nm)[c] | NiO (%)[d] | $Ni^{2+}$ (%)[d] |
|---|---|---|---|---|---|---|---|
| Ni-I | 9.9 | 433 | 0.66 | 5.7 | 13.5 | 80 | 20 |
| CuNi-I | 0.6(Cu), 9.4(Ni) | 451 | 0.66 | 5.6 | 10.7 | 32 | 68 |
| CuNi-PD | 0.5(Cu), 9.5(Ni) | 450 | 0.54 | 4.6 | n.d. | 8 | 92 |

*n.d.* not determined

[a] Metal loading determined by ICP

[b] Specific surface area ($S_g$), pore volume ($V_P$) and average pore diameter ($d_P$) of the calcined samples

[c] Medium NiO crystallite size estimated by Scherrer equation

[d] Fraction of NiO and support-interacting $Ni^{2+}$ species as determined by TPR

monometallic Ni-I sample. Indeed, the total integrated intensity of the peaks in the XRD of CuNi-I was only 43 % of the total integrated intensity measured for Ni-I. It is evident that the addition of a small quantity of $Cu^{2+}$ ions led to a diminution in the amount of NiO crystallites formed on the $SiO_2$–$Al_2O_3$ surface. Even more, when the crystalline domains for both impregnated samples are compared, it can be seen that NiO crystallites in CuNi-I are around 25 % smaller than in Ni-I (Table 1). In the case of the hydrated precursor of CuNi-PD (Fig. 1D), two small and broad peaks are observed at $2\theta = 34.3°$ and 60.7°, which were assigned to a Ni antigorite-like phase ($Ni_3Si_2O_5(OH)_4$, PDF-2-22-0754). This compound, formed by reaction between Ni and support surface, has already been reported for Ni catalysts prepared by precipitation-deposition over $SiO_2$ and $SiO_2$–$Al_2O_3$ [22]. After calcination, this $Ni^{2+}$ compound was partially converted to NiO with very small crystallite size (Fig. 1C). Then, it can be assumed that a highly dispersed $Ni^{2+}$ phase formed by very small crystallites, around 4 nm in size, interacting with the $SiO_2$–$Al_2O_3$ surface was obtained for the CuNi-PD sample. In consequence, it can be stated that the trend for crystallinity degree and crystallite mean size for the three samples is: Ni-I > CuNi-I > CuNi-PD.

TPR profiles of the calcined samples are presented in Fig. 2. The profile of Ni-I sample presents a main $H_2$ consumption peak at 380 °C, that is normally assigned to the reduction of a NiO phase with low or no interaction with the support [17]. A second $H_2$ consumption peak with a maximum at 520 °C and lower intensity than the first one is also observed. This peak is usually assigned to the reduction of a $Ni^{2+}$ phase having a strong interaction with the support [18]. As well, the TPR profile of the CuNi-I sample shows two reduction peaks: the first one at 395 °C and the second one at 505 °C, which are assigned to the same species than in the case of Ni-I. However, in this case, the intensity of both peaks was similar, which indicates that the relative proportion of both species is quite different in both impregnated samples. On the other hand, the TPR profile for CuNi-PD shows only a very broad peak between 300 and 700 °C, with maximum at 520 °C and a small shoulder at 370 °C, that can be assigned to the reduction of a $Ni^{2+}$ phase strongly interacting with the support. This is in agreement with the XRD of CuNi-PD sample, in which the formation of a Ni antigorite-like phase was observed. The absence of the corresponding diffraction lines in the case of CuNi-I could be ascribed to the lower amount of this very highly dispersed phase.

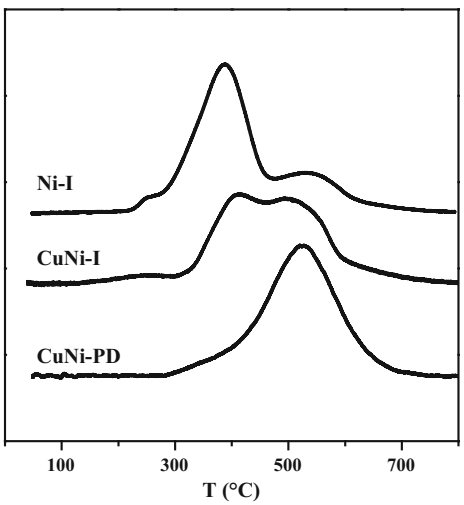


**Fig. 2** Temperature-programmed reduction profiles of oxide precursors calcined in air at 500 °C

In order to estimate the relative proportion of NiO and $Ni^{2+}$ species for each sample, TPR profiles were deconvoluted using two Gaussian peaks, and the corresponding values are shown in Table 1. The NiO:$Ni^{2+}$ proportion shifts from 80:20 for Ni-I to 32:68 for CuNi-I, and to 8:92 for CuNi-PD. It is worth noticing that the ratio of intensities between the NiO reduction peak for CuNi-I and the NiO reduction peak for Ni-I is 40 %, which is in good agreement with the relative intensity obtained from the XRD of these two samples. In consequence, both XRD and TPR results evidence a decrease in the amount of polycrystalline NiO according to the following trend: Ni-I > CuNi-I > CuNi-PD. This trend is jus the opposite to that for the amount of $Ni^{2+}$ phase strongly interacting with support surface. It is then concluded that the addition of a small amount of Cu promotes the interaction of $Ni^{2+}$ ions with the support. These results are in agreement with those obtained in a previous work for CuNi/SBA catalysts [23]. The formation of a strongly interacting $Ni^{2+}$ phase is more favored when the bimetallic sample is prepared by coprecipitation-deposition instead of incipient wetness impregnation.

Ni-I and CuNi-PD were analyzed by TEM, and representative micrographs are shown in Fig. 3. A metallic particle size distribution was obtained for each sample by counting approximately 100 particles from several micrographs; the mean particle size and range are shown in Table 2. A wide distribution of metal particle size was determined for Ni-I sample, which goes from very small particles, around 6 nm, to very large particles, almost 75 nm. On the contrary, very small metal Ni particles in a very narrow range of sizes were observed for CuNi-PD. These two very different particle size distributions can be related, on one hand, with the trend for crystallinity degree and crystallite sizes determined by XRD and, on the other hand, with the trend for the amount of $Ni^{2+}$ phase interacting with the support determined by TPR. In summary, we concluded that reduction of large NiO crystallites having low interaction with the support led to large metal

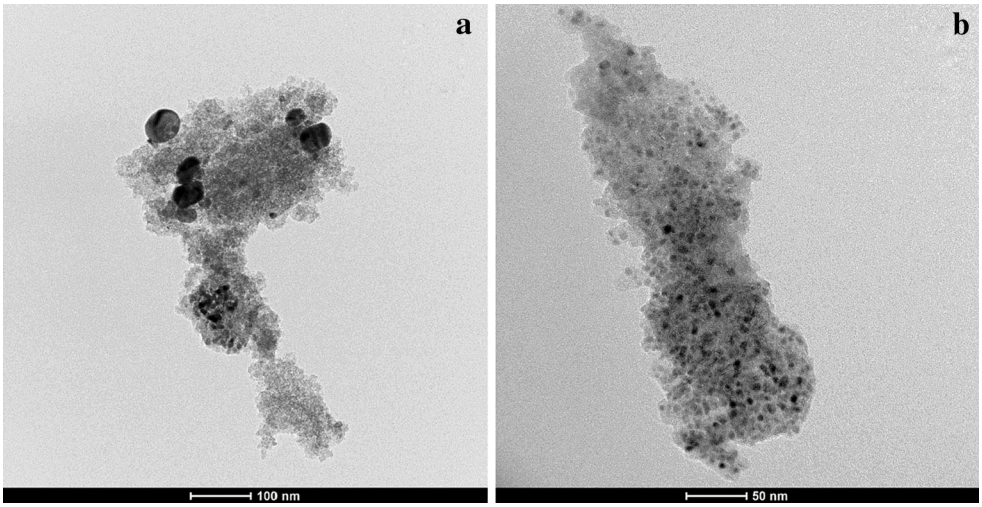


**Fig. 3** TEM images of reduced-passivated samples. **a** Ni-I, **b** CuNi-PD

**Table 2** Hydrogen chemisorption capability and metal particle size of the reduced catalysts

| Sample | CH ($cm^3\ g^{-1}$)[a] | Dp (nm)[b] | DDp (nm)[b] |
|---|---|---|---|
| Ni-I | 0.12 | 26.2 | 6–75 |
| CuNi-I | 0.05 | n.d. | n.d. |
| CuNi-PD | 0.15 | 4.5 | 3–7 |

*n.d.* not determined

[a] Irreversibly chemisorbed hydrogen after reduction at 500 °C

[b] Average $Ni^0$ particle size (Dp) and size range (DDp) determined from TEM micrographs

Ni particles. On the contrary, the reduction of the $Ni^{2+}$ phase strongly interacting with the support gave a metal Ni phase constituted by very small particles. Therefore, the results obtained by TEM are consistent with those obtained by XRD and TPR.

The amount of irreversibly chemisorbed $H_2$ per gram of catalyst (CH) for the reduced catalysts is shown in Table 2. The $H_2$ chemisorption capability for CuNi-I is less than half the one of Ni-I. On the other hand, for CuNi-PD, the volume of chemisorbed hydrogen is three times larger than for CuNi-I and some higher than for Ni-I. These results show that the addition of a small amount of Cu diminishes the hydrogen chemisorption capability of the metal Ni phase. However, the coprecipitation-deposition method leads to a bimetallic catalyst with a higher hydrogen chemisorption capability per gram of sample than the bimetallic sample prepared by impregnation. This is probably due to the fact that the specific metal surface area of CuNi-PD is much larger than that of CuNi-I.

As a summary of the characterization results, it can be stated that the extent of the NiO phase diminishes following the pattern Ni-I > CuNi-I > CuNi-PD, along with a proportional augment of $Ni^{2+}$ ions strongly interacting with the $SiO_2$–$Al_2O_3$ surface. The formation of this $Ni^{2+}$ phase is strongly influenced by the addition of small amounts of $Cu^{2+}$ ions and by the preparation method. The reduction under $H_2$ flow of the low support-interacting NiO phase results in large metallic particles, while the reduction of the strongly support-interacting $Ni^{2+}$ phase yields much smaller bimetallic particles, with intrinsically lower $H_2$ chemisorption capability but higher total metal surface area.

### 3.2 Catalytic Activity

Catalytic tests were carried out at 170, 195 and 220 °C, with a $W/F^0_{AM} = 2$ g h $mol^{-1}$ and under atmospheric pressure. The only products detected in all of the experiments were SA, GBL, PA and $CH_4$. All of the catalysts used in this work were very active for gas phase MA hydrogenation, hence the MA conversions were always close to 100 % and constant during the whole catalytic tests. In a previous paper, under similar conditions as used in this work, we showed that MA is not directly hydrogenolyzed to other products such as GBL or PA, but only hydrogenated to SA, which in turn yields GBL or PA through C=O or C–C and C–O hydrogenolysis, respectively [17]. Then, it is possible to analyze the activity of these catalysts in terms of the SA conversion ($X_{SA}$), calculated as $X_{SA} = (1 - Y_{SA}) \cdot 100$, where $Y_{SA}$ is the mol of SA detected by GC per mol of MA fed, taking into account that total MA conversion was reached [18].

SA conversion as a function of time is shown in Fig. 4 for the three temperatures studied in this work. Ni-I showed no deactivation during the 3 h of catalytic test, reaching

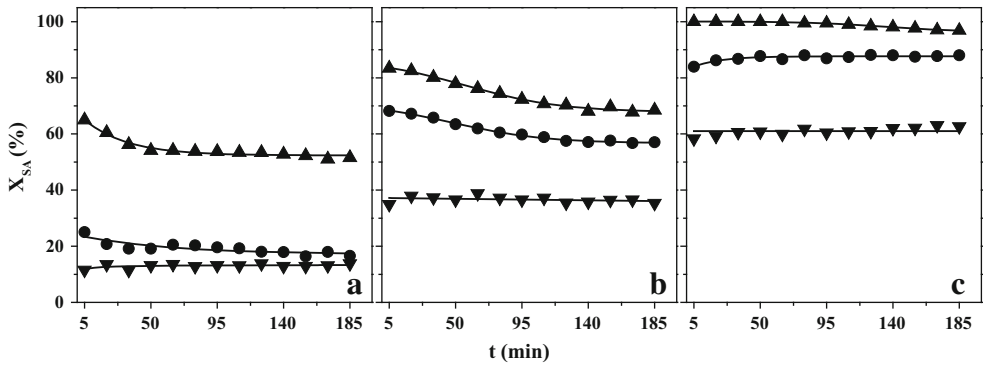


**Fig. 4** Succinic anhydride conversion as a function of time for the (Cu)–Ni/$SiO_2$–$Al_2O_3$ catalysts used in this work at **a** 170 °C, **b** 195 °C, **c** 220 °C. *Filled down pointing triangle* Ni-I, *filled circle* CuNi-I, *filled up pointing triangle* CuNi-PD

conversions of about 15, 38 and 60 % at 170, 195 and 220 °C, respectively. In the case of CuNi-I, SA conversion was always higher than for Ni-I, even though a slight deactivation at 170 and 195 °C was observed. The steady state values (viz. t = 3 h) were 17, 60 and 85 %, at 170, 195 and 220 °C, respectively. The highest SA conversion was reached in all of the cases with CuNi-PD catalyst. The most important difference in catalytic activity between CuNi-PD and catalyst prepared by impregnation was especially observed at the lowest temperature. The initial conversion at 170 °C with CuNi-PD was near 65 %, but during the first hour of reaction the conversion diminished to 55 % and then remained practically constant until the end of the catalytic test. At higher reaction temperatures, the conversion diminished more slowly, dropping from 83 to 73 % at 195 °C and from 100 to 95 % at 220 °C, always reaching an apparent steady state after 3 h.

Comparing the samples prepared by impregnation, Ni-I and CuNi-I, it can be concluded that the addition of a small quantity of Cu increases the hydrogenolytic activity of Ni/$SiO_2$–$Al_2O_3$ catalyst. In the same sense, comparing both bimetallic samples, CuNi-I and CuNi-PD, it can also be concluded that the sample prepared by coprecipitation-deposition is more active for SA hydrogenolysis than the one prepared by impregnation, even though the difference in SA conversion between both bimetallic catalysts became smaller with increasing reaction temperature. In spite of the differences in deactivation behaviour, the hydrogenolytic activity trend was always the following: CuNi-PD > CuNi-I > Ni-I. This pattern is coincident with the one obtained for the amount of $Ni^{2+}$ species strongly interacting with the $SiO_2$–$Al_2O_3$ surface (Table 1), which in turn led to the highly dispersed metal phase observed by TEM. In other words, the trend observed for the SA conversion can be related with an increasing metallic surface area per gram of catalyst as the metal particle size decreases from Ni-I to CuNi-PD. However, it is worth to notice that the increase of initial SA conversion with temperature was considerably

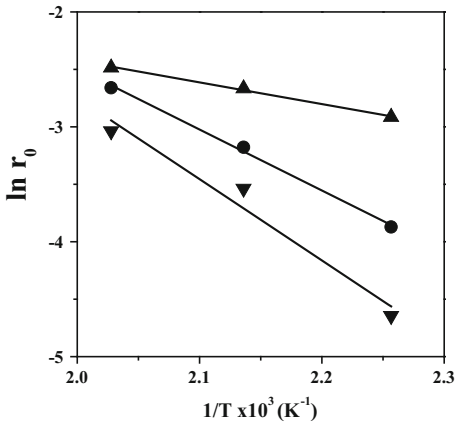


**Fig. 5** Arrhenius plot for the gas phase hydrogenolysis of succinic anhydride over (Cu)–Ni/$SiO_2$–$Al_2O_3$ catalysts. *Filled down pointing triangle* Ni-I, *filled circle* CuNi-I, *filled up pointing triangle* CuNi-PD

smaller for CuNi-PD than for the two catalysts prepared by impregnation (Fig. 4). This is better reflected in an Arrhenius plot, in which natural logarithm of SA hydrogenolysis rate is represented as a function of the reciprocal of reaction temperature (Fig. 5). Then, it is clear that the influence of temperature on SA hydrogenolysis rate with CuNi-PD was much lower than with CuNi-I and Ni-I, which indicates that the apparent activation energy for SA hydrogenolysis should be the lowest for the catalyst prepared by coprecipitation-deposition method. The last would indicate that the metal surface formed from the reduction of a $Ni^{2+}$ phase strongly interacting with $SiO_2$–$Al_2O_3$ is more active for SA adsorption and subsequent selective hydrogenolysis into GBL than the surface obtained by reduction of large NiO crystallites. Therefore, the pattern obtained for the SA hydrogenolysis rate can be explained on the basis of both an increase of total metal surface and structural changes on the metal surface, due to the addition of small amounts of Cu and the preparation method.

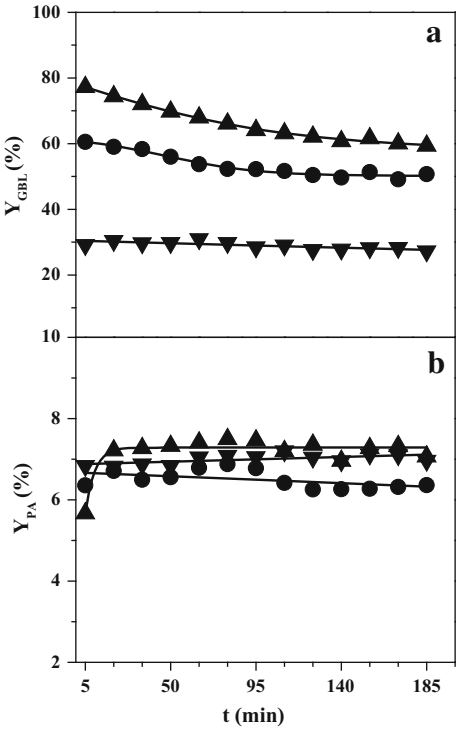


**Fig. 6** Yields in γ-butyrolactone (**a**) and propionic acid (**b**) as a function of time for the (Cu)–Ni/$SiO_2$–$Al_2O_3$ catalysts used in this work at 195 °C. *Filled down pointing triangle* Ni-I, *filled circle* CuNi-I, *filled up pointing triangle* CuNi-PD

The curves of GBL yield as a function of time are similar to those obtained for the corresponding curves of SA conversion. As an example, the yield in GBL as a function of time at 195 °C with the three catalysts is shown in Fig. 6a. When these curves are compared with those obtained for SA conversion at the same temperature (Fig. 4b), the same trend is observed: CuNi-PD > CuNi-I > Ni-I. The yield in PA was always approximately constant with reaction time and lower than 10 %, being around 7 % at 195 °C (Fig. 6b). Besides, at each temperature, the yield in PA was very similar for the three catalysts. On the other hand, $CH_4$, which is a byproduct of GBL hydrogenolysis to PA, was always present in very low yields (from 0.5, at 170 °C, to 2 %, at 220 °C), which indicates that almost all PA was produced from SA hydrogenolysis [17].

In summary, MA was easily hydrogenated to SA in gas phase on Ni(Cu)/$SiO_2$–$Al_2O_3$ catalysts and then SA was mainly converted into GBL by selective hydrogenolysis of C=O bond. Only a minor amount of SA was converted to PA through hydrogenolysis of C–C and C–O bonds. Finally, negligible amounts of GBL are hydrogenolyzed to PA and $CH_4$. This complex reaction network is represented in Scheme 1.

As we pointed out above, while GBL yield diminished with time probably due to deactivation of active sites, PA

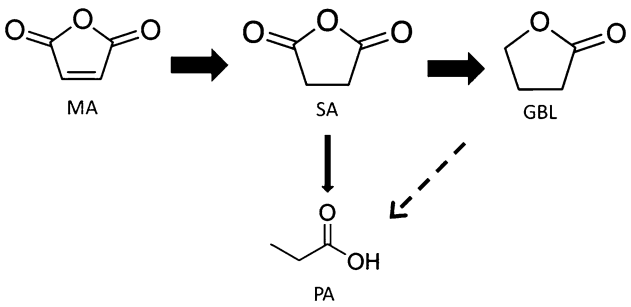


**Scheme 1** Reaction network for maleic anhydride hydrogenation under the conditions used in this work. *MA* maleic anhydride, *SA* succinic anhydride, *GBL* γ-butyrolactone, *PA* propionic acid

yield kept almost constant (Fig. 6). These differences in the time evolutions for the yields in GBL and PA were explained in a previous work considering the coexistence of two different types of hydrogenolytic sites on the metal surface [17], one of them active in the hydrogenolysis of SA to GBL and the other one active in the hydrogenolysis of SA to PA. The metal sites that are active in the hydrogenolysis of SA to GBL are deactivated faster than those active in the hydrogenolysis of SA to PA, probably due to strong adsorption of reactant and/or product molecules. According to the results presented in this work, the adsorption of reactant and/or product molecules is stronger on Cu-modified Ni/$SiO_2$–$Al_2O_3$ catalysts than on Ni-I catalyst. This can be explained considering that reduction of support-interacting $Ni^{2+}$ species leads to metal Ni sites that can adsorb product and/or reactant molecules more strongly than metal Ni phase obtained by reduction of NiO. As CuNi precursors have a higher proportion of $Ni^{2+}$ species strongly interacting with support respect to NiO, then a higher deactivation would be expected for bimetallic CuNi catalysts than for Ni-I catalyst, even at similar conversions levels (Fig. 4). The diminution of deactivation effect with temperature can be explained by considering that adsorption strength of reactants and/or products diminishes and the hydrogenation rate of these strongly adsorbed species increases as the reaction temperature is raised [16]. This effect is more pronounced in the case of CuNi-PD than in the case of CuNi-I, which is consistent with the low apparent activation energy observed for this sample (Fig. 5).

In order to neglect the effect of deactivation, the initial selectivity to GBL, defined as: $S^0_{GBL} = Y^0_{GBL}/\left(Y^0_{GBL} + Y^0_{PA}\right)$ and the initial and final yields $\left(Y^0_{GBL}, Y^F_{GBL}\right)$ in GBL at 170 and 220 °C are shown in Fig. 7 for the three catalysts. Selectivities to GBL close to 90 % and GBL yields of 80–85 % were reached with the bimetallic samples at a reaction temperature of 220 °C. It is worth to notice that GBL yields of only 45 % or lower were reported when the gas phase MA hydrogenation was carried out over Ni-

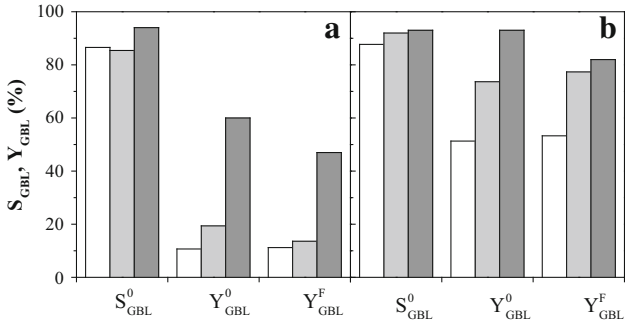


**Fig. 7** Initial GBL selectivity $(S^0_{GBL})$, and initial and final GBL yield $(Y^0_{GBL}, Y^F_{GBL})$, at **a** 170 °C and **b** 220 °C. *White* Ni-I, *light grey* CuNi-I, *dark grey* CuNi-PD

based catalysts [24–26]. Moreover, these yields in GBL were reached only over Pt-doped $Ni/Al_2O_3$ catalysts at pressures higher than 10 bar [24]. Then, catalytic results presented in this work are clearly superior to the as yet reported in the literature, including our previous works with $Ni/SiO_2$ [17].

It is observed that CuNi-PD was slightly more selective to GBL than Ni-I and CuNi-I, mainly at 170 °C. Besides, for similar levels of SA conversion, almost the same selectivity to GBL was obtained with Ni-I and CuNi-I catalysts at 170 °C (Figs. 4a, 7a) and also with CuNi-I and CuNi-PD at 195 and 220 °C (Figs. 4b, c, 7b). The initial and final yields to GBL, both at 170 and 220 °C, followed the same trend observed for GBL yield at 195 °C (Fig. 6a). Even more, at each temperature, GBL yields are similar to the corresponding SA conversions (Figs. 4, 7). This indicates that as the metal particle size became smaller, the SA conversion and GBL yield increased while only small changes in SA selectivity were observed. Then, the main effect of obtaining a metal phase constituted by smaller particles is an increase in the number of hydrogenolytic sites per gram of catalyst, which leads to an important rise in the global rate for SA hydrogenolysis. However, the highest selectivity to GBL with CuNi-PD at 170 °C indicates that the ratio of surface sites active for SA hydrogenolysis to GBL respect to those for SA hydrogenolysis to PA is some higher on the metal surface of CuNi-PD than of Ni-I and CuNi-I. This statement is in line with structural differences suggested from the variations in SA hydrogenolysis rate observed with temperature (Fig. 5).

The trend for deactivation is following the same pattern as for hydrogenolytic activity: CuNi-PD > CuNi-I > Ni-I. This indicates that the active sites on the surface of the smallest particles can chemisorb more strongly reactant and/or product molecules than those on the larger metal particles. Therefore, this is also in agreement with some structural changes that occur on the metal Ni surface due to addition of small amounts of Cu and the preparation method.

In summary, two main outcomes can be inferred from the experimental results obtained: (1) the addition of small amounts of Cu and the use of coprecipitation-deposition method lead to an important increase of the SA hydrogenolysis rate and GBL yield, probably due to the increasing number of surface hydrogenolytic sites per gram of catalyst as the metal particle size decreases; (2) the preparation of $Cu–Ni/SiO_2–Al_2O_3$ by coprecipitation-deposition promotes some surface structural changes that lead to a decrease of the apparent activation energy and to an increase in selectivity to GBL.

## 4 Conclusions

Gas-phase MA hydrogenation was studied on Cu-modified Ni catalysts supported on $SiO_2–Al_2O_3$. It was found that both the addition of a small quantity of Cu and the preparation method greatly affect the physicochemical characteristics of the catalysts, as well as its catalytic performance. Specifically, adding a small amount of $Cu^{2+}$ ions to the precursor favours the formation of a $Ni^{2+}$ phase that interacts strongly with the support surface, in detriment of the large NiO crystallites formed on $Ni/SiO_2–Al_2O_3$ catalyst. Preparation of the $Cu–Ni/SiO_2–Al_2O_3$ catalyst by the coprecipitation-deposition method, instead of incipient wetness impregnation, enhances the formation of this oxide phase strongly interacting with the support. The reduction of the low support-interacting NiO phase results in large metallic particles, while the reduction of the strongly support-interacting $Ni^{2+}$ phase yields smaller metallic particles, with intrinsically lower $H_2$ chemisorption capability but a much higher specific surface metal area.

The metallic Ni phase obtained from the reduction of the $Ni^{2+}$ phase is more active in the selective SA hydrogenolysis to γ-butyrolactone than the one formed from NiO phase reduction. This was attributed to the higher specific metallic surface area and to some probable structural changes on the metal Ni surface. Both effects lead to a very important increase of the yield in GBL respect to the metal phase obtained from the reduction of large NiO crystallites.

Both the effect of the addition of small amounts of Cu to Ni and the use of coprecipitation-deposition method make $Cu–Ni/SiO_2–Al_2O_3$ the best catalyst in this work for γ-butyrolactone production from MA under $H_2$ gas flow.

**Acknowledgments** We thank the Universidad Nacional del Litoral (UNL), Consejo Nacional de Investigaciones Científicas y Técnicas (CONICET) and Agencia Nacional de Promoción Científica y Tecnológica (ANPCyT) from Argentina for the financial support of this work. We also acknowledge to LMA-INA-UNIZAR facilities for the transmission electronic microscopy analyses.

## References


1. Zhang B, Zhu Y, Ding G, Zheng H, Li Y (2012) Appl Catal A Gen 44:191–201
2. Yu Y, Guo Y, Zhan W, Guo Y, Wang Y, Wang Y, Zhang Z, Lu G (2011) J Mol Catal A Chem 337:77–81
3. Budroni G, Corma A (2008) J Catal 257:403–408
4. Messori M, Vaccari A (1994) J Catal 150:177–185
5. Zhang R, Yin H, Zhang D, Qi L, Lu H, Shen Y, Jiang T (2008) Chem Eng J 140:488–496
6. Gao D, Feng Y, Yin H, Wang A, Jiang T (2013) Chem Eng J 233:349–359
7. Castiglioni GL, Vaccari A, Fierro G, Inversi M, Lo Jacono M, Minelli G, Pettiti I, Porta P, Gazzano M (1995) Appl Catal A Gen 123:132–144
8. Zhu YL, Yang J, Dong GQ, Zheng HY, Zhang HH, Xiang HW, Li YW (2005) Appl Catal B Environ 57:183–190
9. Yu Y, Guo Y, Zhan W, Guo Y, Wang Y, Lu G (2014) J. Mol Catal A Chem 392:1–7
10. Regenhardt SA, Trasarti AF, Meyer CI, Garetto TF, Marchi AJ (2013) Catal Commun 35:59–63
11. Vaidya SH, Rode CV, Chaudhari RV (2007) Catal Commun 8:340–344
12. Jung SM, Godard E, Jung SY, Park KC, Choi JU (2003) J Mol Catal A Chem 198:297–302
13. Lu W, Lu G, Guo Y, Guo Y, Wang Y (2003) Catal Commun 4:177–181
14. Ohlinger C, Kraushaar-Czarnetzki B (2003) Chem Eng Sci 58:1453–1461
15. Marchi AJ, Fierro JLG, Santamaria J, Monzon A (1996) Appl Catal A Gen 142:375–386
16. Meyer CI, Marchi AJ, Monzon A, Garetto TF (2009) Appl Catal A Gen 367:122–129
17. Meyer CI, Regenhardt SA, Marchi AJ, Garetto TF (2012) Appl Catal A Gen 417–418:59–65
18. Regenhardt SA, Meyer CI, Garetto TF, Marchi AJ (2012) Appl Catal A Gen 449:81–87
19. Meyer CI, Regenhardt SA, Bertone ME, Marchi AJ, Garetto TF (2013) Catal Lett 143:1067–1073
20. Geus JW, van Dillen AJ (2008) In: Ertl G, Knözinger H, Schüth F, Weitkamp J (eds) Handbook of heterogeneous catalysis, VCH, Weinheim
21. Montes M, Penneman de Bosscheyde C, Hodnett BK, Delannay F, Grange P, Delmon B (1984) Appl Catal 12:309–330
22. Gil A, Díaz A, Gandía LM, Montes M (1994) Appl Catal A Gen 109:167–179
23. Habimana F, Li X, Ji S, Lang B, Sun D, Li C (2009) J Nat Gas Chem 18:392–398
24. Li J, Tian WP, Wang X, Shi L (2011) Chem Eng J 175:417–422
25. Guo S, Shi L (2013) Catal Today 212:137–141
26. Huo W, Zhang C, Yuan H, Jia M, Ning C, Tang Y, Zhang Y, Luo J, Wang Z, Zhang W (2014) J Ind Eng Chem 20:4140–4145